Far-field sound radiation due to an installed open rotor

by

A. McAlpine and M.J. Kingan

reprinted from

international journal of

aeroacoustics

volume 11 · number 2 · 2012

published by MULTI-SCIENCE PUBLISHING CO. LTD.,
5 Wates Way, Brentwood, Essex, CM15 9TB UK
E-MAIL: mscience@globalnet.co.uk
WEBSITE: www.multi-science.co.uk

International Journal of aeroacoustics volume 11 · number 2 · 2012– pages 213 – 245

Far-field sound radiation due to an installed open rotor

A. McAlpine and M.J. Kingan

Institute of Sound and Vibration Research, University of Southampton, Southampton, SO17 1BJ, UK
email: am@isvr.soton.ac.uk

Received Feb. 4, 2011; Revised March 7, 2011; Accepted April 28, 2011

ABSTRACT

Future single rotation propeller and contra-rotating advanced open rotor concepts promise a significant fuel efficiency advantage over current generation turbofan engines. The development of rotors which produce a minimum level of noise is a critical technical issue which needs to be resolved in order for these concepts to become viable aircraft propulsors. Noise and emissions are subject to stringent legislative requirements, thus accurate models are required in order to predict the noise radiated from aircraft engines. In this article, the development of a theoretical model to predict noise levels of an installed open rotor is reported. First a canonical problem is examined: how to predict the pressure field produced by a rotating ring of point sources adjacent to a rigid cylinder. Analytic expressions for the far-field pressure from a rotating ring of single-frequency monopole and dipole point sources, located near an infinitely long rigid cylinder, immersed in a constant axial mean flow, are explicitly formulated. Illustrative results show how the far-field pressure is affected by varying the source rotational direction, source location and source radius. Next the solution of the canonical problem is utilized to formulate a more advanced model to predict the noise due to an installed open rotor. In this model, the rotor noise sources are represented by a distribution of rotating sources. The adjacent aircraft fuselage is modeled by the rigid cylinder, and the effect of the fuselage boundary layer and other steady distortions are neglected. Also neglected is the scattering from other surfaces such as the pylon, wing and centerbody. This distributed source model can be used to calculate the effect of scattering of open rotor noise by an adjacent cylindrical fuselage. The model can be used to calculate both rotor-alone tones and tones produced by periodic unsteady loading on the rotor blades. Practical examples are provided which show how the effect of blade rotational direction and propeller location relative to the fuselage affect the sound produced by the interaction of a pylon wake with a rotor in a pusher configuration.

1. INTRODUCTION

Noise and emissions are critical technical issues in the development of aircraft engines, and are subject to stringent legislative requirements. Currently, there is renewed interest in open rotor, contra-rotating propellers, which are more fuel efficient than comparable high-bypass ratio turbofan engines. Owing to the interaction of each rotor with the unsteady flow-field produced by the adjacent contra-rotating rotor, the radiated sound pressure will consist of a multitude of tones at frequencies equal to integer multiples of

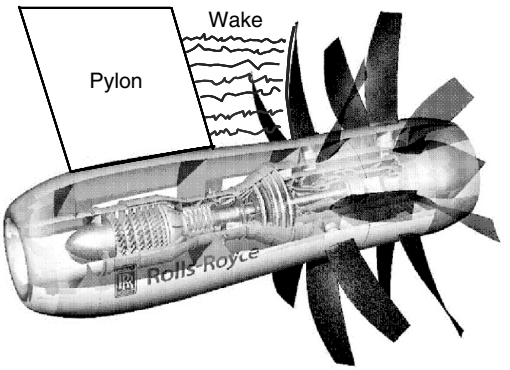

Figure 1: Advanced open rotor concept in pusher configuration (courtesy of Rolls-Royce plc).

the sum and difference of the front and rear rotor blade passing frequencies. Also the open rotor will be attached either to the fuselage or the wing, using a large pylon, as shown in figure 1. The pylon will attach to the open rotor centerbody either upstream (pusher configuration) or downstream (puller configuration) of the rotor blades. For engines mounted in a pusher configuration, the interaction of the wake produced by the upstream pylon with the rotor blades will induce unsteady loading on the rotor blades which in turn will produce tones at integer multiples of the rotor's blade passing frequency. The minimization of the tonal noise is a critical technical issue which needs to be met if open rotors are to be introduced into civil aviation.

The objective of the work reported in this article[†] is to provide a theoretical model which can be used to investigate installation effects for an open rotor. First a canonical problem which is a simple representation of an installed open rotor is examined. In this 'point source' model, rotor noise sources are represented in terms of idealised rotating point sources. Subsonically rotating, single-frequency, monopole and dipole point sources are considered. The adjacent aircraft fuselage is represented by an infinitely long rigid cylinder. Taking an infinite cylinder avoids having to develop a solution that includes scattering and diffraction at the cylinder's ends. Also, a constant mean flow in a direction aligned with the axis of the cylinder is included in the model problem. Taking uniform flow means that the effect of the fuselage boundary layer is omitted in the current analysis[‡].

[†]This work was presented at the 14th CEAS-ASC Workshop (& 5th Scientific Workshop of X3-Noise) on Aeroacoustics of high-speed aircraft propellers and open rotors, Institute of Aviation, Warsaw, Poland, 7–8 October 2010.

[‡]The inclusion of the boundary layer would require a solution (in this region) of the linearized Euler equations or the Pridmore-Brown equation, in which case it would not be possible to obtain a closed form analytic solution.

Next the 'point source' model is extended in order to account for a distribution of monopole and dipole sources over the surface of each blade of an open rotor. The 'distributed source' model is then used to calculate the effect of scattering of open rotor tones by an adjacent cylindrical fuselage.

The model can be used to calculate the pressure due to both rotor-alone tones and interaction tones. Rotor-alone tones are produced by the steady loading on, and finite thickness of, the rotor blades. Interaction tones are produced by the periodic loading on the rotor blades caused by their interaction with, for example, the wakes or potential field of an adjacent rotor or pylon. Particular attention is given to the scattering of tones produced by the interaction of the wake from an upstream pylon with the front rotor. Rotor-alone tones (thickness and steady loading) can be represented by monopole and dipole sources with source strength independent of position and time, whereas interaction tones (unsteady loading) can be represented by dipole sources with periodic variation in source strength[§].

The approach herein follows the procedure outlined in Hanson and Magliozzi [1], albeit the effect of the fuselage boundary layer is not included in the current work. In Ref. [1] the incident field due to a propeller noise source in free space is utilized to determine the total field in the presence of an aircraft fuselage which is modelled by an infinite, rigid cylinder. The incident field is given by near-field frequency-domain propeller source theory developed previously by Hanson. This solution was derived in a coordinate system centred on the propeller. Accordingly, in Ref. [1] the authors show how to shift the solution to a coordinate system which is centred on the axis of the cylinder, using Graf's Addition theorem. They then combine this with an appropriate form of the scattered field (a sum of outward propagating cylindrical waves): the resultant sum of the incident and scattered fields gives the total pressure field. Their analysis also includes the effect of the fuselage boundary layer, and they match their analytical solutions to a numerical solution in the boundary layer. The methodology utilized in the present work is essentially the same as that proposed by Hanson and Magliozzi. However, in Ref. [1] the authors do not give analytical solutions formulated explicitly for rotating, single-frequency, monopole and dipole point sources, or their far-field approximations.

A comprehensive aeroacoustic study into propeller noise has been reported by Whitfield, Gliebe, Mani and Mungur [2] for single-rotation propellers, and by Whitfield, Mani and Gliebe [3] for counter-rotating propellers. In the former report, there are detailed sections on installation effects and scattering of propeller noise by the aircraft fuselage and wings. Their modelling of the scattering of propeller noise by a cylindrical fuselage follows essentially the same method as that proposed by Hanson and Magliozzi [1].

Also, Fuller [4] has examined the scattering of spherical waves by an infinite, rigid cylinder, and how the sound radiation levels are affected by the presence of the cylinder.

[§]Broadband (incoherent) sources would require a solution which permits the source strength to vary randomly with time: this type of source has not been included in the analysis.

He examined the field due to stationary monopole and dipole point sources located near a cylinder, also using the type of approach followed by Hanson and Magliozzi [1], albeit for stationary sources only. In fact the solution for a monopole point source located near an infinite, rigid cylinder has been known for many years, and is given in the text on Electromagnetic and Acoustic Scattering by Simple Shapes by Bowman, Senior and Uslenghi [5], published in 1969.

Unpublished recent work by Leppington, Blakemore and Heron [6] examines the same canonical problem which is considered in this article. The authors solve the problem following an alternative procedure from previous work in Refs. [1, 2, 4]. Leppington, Blakemore and Heron solve the convected wave equation for a point source, but take a reference frame which is centred on the axis of the cylinder. The wave equation is solved using Fourier transform methods. The resulting solution does not need to be shifted to a different reference frame. However, their solution appears more complex compared to the solution presented in this paper.

A related problem has been investigated by Glegg [7], and more recently by Kingan, Powles and Self [8]. This problem involves the effect of centrebody scattering on propeller noise. The key difference in the mathematical formulation between this problem, and the problem of fuselage scattering, is that in the former problem, the axis of the propeller and the axis of the centrebody are coincident, which avoids the need to shift the near-field solution of the propeller to a new reference frame. This shift of coordinate systems, achieved using Graf's Addition theorem, significantly alters the subsequent analysis. Other examples of related work include Hanson [9], Lu [10] and Kopiev, Maslov and Chernyshov [11]. Similar to Hanson and Magliozzi [1], these articles all concern the effect of shielding by the fuselage boundary layer. In the work reported in this article, the effect of the fuselage boundary layer and other steady distortions are neglected. Also neglected is the scattering from other surfaces such as the pylon, wing and centerbody.

2. POINT SOURCE MODEL

A sketch of the canonical problem set-up is shown in figure 2. The point source moves along a helical path, centred on an axis of rotation which lies parallel to the axis of the cylinder. The axis of rotation lies a horizontal distance of $b\cos\beta$ and a vertical distance of $b\sin\beta$ from the axis of the cylinder. The radius of the helical path is a, and the radius of the cylinder is a_0, where $a + a_0 < b$. The angular velocity of the point source is Ω and its axial velocity is U. The cylinder is of infinite length and is rigid.

In a uniform, stationary medium with constant sound speed c_0 and density ρ_0, from the Ffowcs Williams-Hawkings equation, the acoustic pressure field $p'(\mathbf{x}, t)$ due to a monopole or dipole source is given by the solution of the inhomo-geneous wave equation

$$\left(\nabla^2 - \frac{1}{c_0^2}\frac{\partial^2}{\partial t^2}\right)p' = s(\mathbf{x},t) \quad \text{where} \quad s(\mathbf{x},t) = -\rho_0\frac{\partial q}{\partial t} \quad \text{or} \quad \nabla\cdot\mathbf{f}. \tag{1}$$

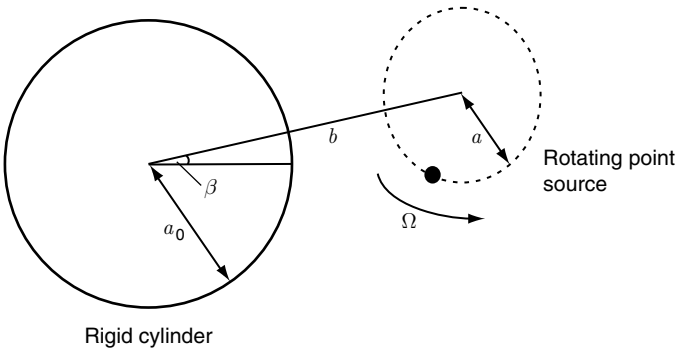

Figure 2: Sketch of canonical installed open rotor problem.

For a monopole source, $s = -\rho_0 \partial q/\partial t$, where $q(\mathbf{x},\ t)$ is the volume flow rate per unit volume, or for a dipole source $s = \nabla \cdot \mathbf{f}$, where $\mathbf{f}\,(\mathbf{x},\ t)$ is the force per unit volume. Only single-frequency, subsonic sources are considered. Since the sources are moving then,

$$q(\mathbf{x},t) = Q_0 e^{i\omega_0 t}\delta(\mathbf{x} - \mathbf{X}(t)) \quad \text{and} \quad \mathbf{f}(\mathbf{x},t) = \mathbf{F}_0 e^{i\omega_0 t}\delta(\mathbf{x} - \mathbf{X}(t)), \tag{2}$$

where $\mathbf{X}(t)$ denotes the position of the source at time t, Q_0 is volume velocity and $\mathbf{F}_0$ is force.

The solution method is as follows. First, the incident pressure field p_i' due to a rotating, single-frequency, monopole or dipole point source is determined using Fourier transform methods. This is the pressure field that would be present in the absence of the cylinder. It is convenient to determine the incident field in terms of a moving reference frame, $(x,\ y,\ z) = (r\ \cos\ \phi,\ r\ \sin\ \phi,\ z)$, centred on the source's axis of rotation. In this moving frame, the source is located in the plane $z = 0$, and there is a mean axial flow with velocity $-U$ in the positive z-direction. The subsequent analysis then follows the method proposed by Hanson and Magliozzi [1]. The solution for the incident field is shifted, using Graf's Addition theorem, so that the expression is given in terms of another moving reference frame, $(\bar{x},\ \bar{y},\ \bar{z}) = (\bar{r}\ \cos\ \bar{\phi},\ \bar{r}\ \sin\ \bar{\phi},\ \bar{z})$, centred on the axis of the cylinder. (Note that $z \equiv \bar{z}$.) The incident field impinging on a solid object produces scattered waves. An appropriate form of the scattered pressure field p_s' is found. This is related to the shape of the scattering object. In this case the scattered field is expressed in terms of outward propagating cylindrical waves. The total pressure field p_t' is the sum of the incident and scattered fields, $p_i' + p_s'$. This is the pressure field with the cylinder located near the rotating source. The total pressure field is deduced so that it satisfies appropriate boundary and radiation conditions. Finally, the total pressure field in the far field is found by an asymptotic evaluation of the inverse Fourier transform, using the method of stationary phase. The canonical problem set-up, including the moving coordinate systems, is shown in figure 3.

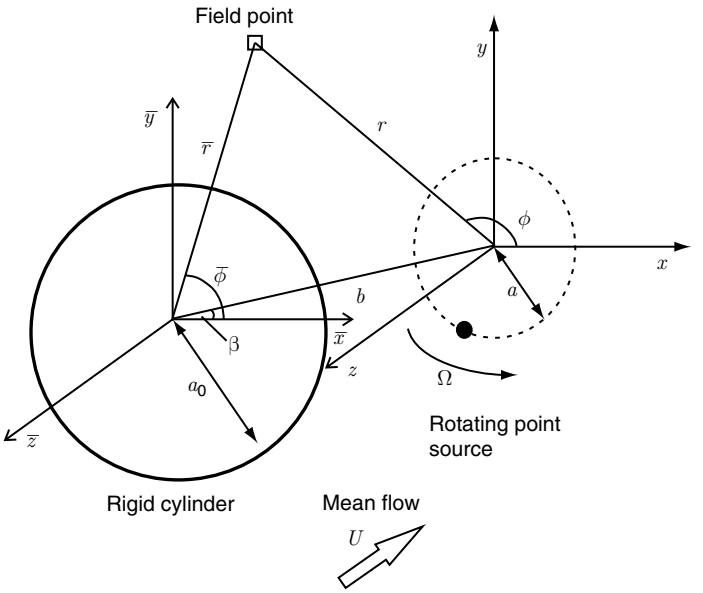

Figure 3: Sketch of canonical installed open rotor problem including the source and cylinder coordinate systems.

2.1. Incident field

The incident field for a rotating, single-frequency, monopole source is found by solving

$$\frac{\partial^2 p_i'}{\partial r^2}+\frac{1}{r}\frac{\partial p_i'}{\partial r}+\frac{1}{r^2}\frac{\partial^2 p_i'}{\partial \phi^2}+\frac{\partial^2 p_i'}{\partial z^2}-\frac{1}{c_0^2}\left(\frac{\partial}{\partial t}-U\frac{\partial}{\partial z}\right)^2 p_i'=-\rho_0\left(\frac{\partial}{\partial t}-U\frac{\partial}{\partial z}\right)q, \quad (3)$$

where

$$q(r,\phi,z,t)=Q_0 e^{i\omega_0 t}\,\frac{\delta(r-a)}{r}\left(\sum_{n=-\infty}^{\infty}\delta(\phi-\Omega t-2\pi n)\right)\delta(z), \quad (4)$$

and the position of the point source is $r=a$, $\phi=\Omega t$ and $z=0$.

The solution of equation (3) is found using Fourier transform methods. Introduce the Fourier transform in z and t, and the Fourier series in ϕ as follows:

$$\widetilde{p'}_m(r,k_z,\omega)=\int_{-\infty}^{\infty}\int_{-\pi}^{\pi}\int_{-\infty}^{\infty}p'(r,\phi,z,t)\,e^{i(k_z z+m\phi-\omega t)}dz\,d\phi\,dt, \quad (5)$$

$$\Rightarrow \quad p'(r,\phi,z,t) = \frac{1}{(2\pi)^3} \sum_{m=-\infty}^{\infty} \left(\int_{-\infty}^{\infty} \int_{-\infty}^{\infty} \widetilde{p'}_m(r,k_z,\omega) e^{-i(k_z z - \omega t)} dk_z d\omega \right) e^{-im\phi}, \quad (6)$$

where k_z, m and ω denote the axial wavenumber, azimuthal order and angular frequency, respectively.

This transforms derivatives as follows:

$$\frac{\partial}{\partial z} \rightarrow -ik_z, \quad \frac{\partial}{\partial \phi} \rightarrow -im \quad \text{and} \quad \frac{\partial}{\partial t} \rightarrow i\omega. \quad (7)$$

Transforming the inhomogeneous wave equation (3) following (5) leads to

$$\frac{d^2 \widetilde{p'}_{im}}{dr^2} + \frac{1}{r} \frac{d\widetilde{p'}_{im}}{dr} + \left\{ (k + k_z M)^2 - k_z^2 - \frac{m^2}{r^2} \right\} \widetilde{p'}_{im} = \mathcal{Q}_m, \quad (8)$$

where

$$\mathcal{Q}_m = -iQ_0 \rho_0 c_0 (k + k_z M) \frac{2\Omega(-1)^{m+1} \sin \pi \left(\dfrac{\omega - \omega_0}{\Omega} \right)}{m\Omega - [\omega - \omega_0]} \frac{\delta(r-a)}{r} \sum_{n=-\infty}^{\infty} \delta(\omega - [\omega_0 + n\Omega]), \quad (9)$$

and $k = \omega / c_0$, $M = U / c_0$.

The solution of equation (8) can be obtained using the method of variation of parameters. Taking $\mathcal{Q}_m = 0$, then (8) is in the form of Bessel's differential equation, i.e.

$$\frac{d^2 \widetilde{p'}_{im}}{dr^2} + \frac{1}{r} \frac{d\widetilde{p'}_{im}}{dr} + \left\{ \Gamma^2 - \frac{m^2}{r^2} \right\} \widetilde{p'}_{im} = 0, \quad (10)$$

where the 'radial' wavenumber Γ is defined as

$$\Gamma^2 = (k + k_z M)^2 - k_z^2. \quad (11)$$

It is convenient† to take $J_m(\Gamma r)$ and $H_m^{(2)}(\Gamma r)$ as the linearly independent solutions of Bessel's differential equation. Then the solution of equation (8) is

$$\begin{aligned}\widetilde{p'}_{im} = J_m(\Gamma r)\left(A_m(k_z,\omega) - i\frac{\pi}{2}\int_0^r \mathcal{Q}_m(s)H_m^{(2)}(\Gamma s)s\,ds\right) + \\ H_m^{(2)}(\Gamma r)\left(B_m(k_z,\omega) + i\frac{\pi}{2}\int_0^r \mathcal{Q}_m(s)J_m(\Gamma s)s\,ds\right),\end{aligned} \tag{12}$$

where A_m and B_m are functions of k_z and ω only, and s is a dummy integration variable.

After inserting $\mathcal{Q}_m$ (9) into $\widetilde{p'}_{im}$ (12), and evaluating the integrals, then the functions A_m and B_m can be found by applying appropriate finiteness and radiation conditions, in the limit as $r \to 0$ and $r \to \infty$, respectively. The resulting solution can be expressed in the form

$$\begin{aligned}\widetilde{p'}_{im}(r,k_z,\omega) = \frac{\pi}{2}Q_0\rho_0 c_0(k+k_z M)\frac{2\Omega(-1)^{m+1}\sin\pi\left(\dfrac{\omega-\omega_0}{\Omega}\right)}{m\Omega-[\omega-\omega_0]} \\ \left(\sum_{n=-\infty}^{\infty}\delta(\omega-[\omega_0+n\Omega])\right)\times H_m^{(2)}(\Gamma r>)J_m(\Gamma r<),\end{aligned} \tag{13}$$

where $r>$ and $r<$ are defined as follows:

$$r>=\begin{cases} r, & r>a \\ a, & r<a \end{cases} \quad \text{and} \quad r<=\begin{cases} a, & r>a \\ r, & r<a \end{cases}. \tag{14}$$

Now define

$$\overline{p'}_{im}(r,k_z,t) = \frac{1}{2\pi}\int_{-\infty}^{\infty}\widetilde{p'}_{im}(r,k_z,\omega)e^{i\omega t}d\omega, \tag{15}$$

which is the inverse Fourier time-transform. The ω-integration can be performed by noting that the zeros of the delta-function in equation (13) occur when $\omega = \omega_0 + n\Omega$. Thus, the solution for $\overline{p'}_{im}$ is given by

†Taking $H_m^{(2)}(\Gamma r)$ in place of $Y_m(\Gamma r)$ will simplify the analysis when applying the radiation condition as $r \to \infty$.

$$\overline{p'}_{im}(r,k_z,t)=\frac{\pi}{2}Q_0\rho_0c_0(k_{0m}+k_zM)H_m^{(2)}(\Gamma_{0m}r>)J_{\boldsymbol{m}}(\Gamma_{0m}r<)e^{i(\omega_0+m\Omega)t}, \quad (16)$$

where k_{0m} and Γ_{0m} are defined as

$$k_{0m}=\frac{\omega_0+m\Omega}{c_0} \quad \text{and} \quad \Gamma_{0m}^{\ 2}=(k_{0m}+k_zM)^2-k_z^2. \quad (17)$$

Also, on comparing the definition of Γ (11) with $\overline{p'}_{im}$ (16), in order to ensure that only outward propagating waves are allowed as $r\to\infty$, then

$$\Gamma_{0m}=\begin{cases}\operatorname{sgn}(\omega_0+m\Omega)\sqrt{(k_{0m}+k_zM)^2-k_z^2}, & (k_{0m}+k_zM)^2>k_z^2\\ -i\gamma_{0m} \quad \text{where} \quad \gamma_{0m}=\sqrt{k_z^2-(k_{0m}+k_zM)^2}, & (k_{0m}+k_zM)^2<k_z^2\end{cases}, \quad (18)$$

which ensures that the correct sign of the square root is selected, depending whether the angular frequency $(\omega_0+m\Omega)$ is positive or negative.

A similar analysis can be performed for a rotating dipole source. The three components of the force $\mathbf{F}_0=(F_{0r},\,F_{0\phi},\,F_{0z})$ correspond to a 'radial', 'angular' and 'axial' dipole, respectively. In the context of sound radiation from an open rotor, only the contributions from the 'angular' and 'axial' dipoles are significant, so in the following analysis the contribution of the 'radial' dipole is omitted by setting $F_{0r}=0$. For the rotating dipole source, the incident field is found to be

$$\overline{p'}_{im}(r,k_z,t)=\frac{\pi}{2}\left(\frac{m}{a}F_{0\phi}+k_zF_{0z}\right)H_m^{(2)}(\Gamma_{0m}r>)J_m(\Gamma_{0m}r<)e^{i(\omega_0+m\Omega)t}. \quad (19)$$

The results for the monopole and dipole sources are now summarized as follows. The incident field due to a rotating point source is given by

$$p_i'(r,\phi,z,t)=\frac{1}{(2\pi)^2}\sum_{m=-\infty}^{\infty}\left(\int_{-\infty}^{\infty}\overline{p'}_{im}(r,k_z,t)e^{-ik_zz}dk_z\right)e^{-im\phi}, \quad (20)$$

where

$$\overline{p'}_{im}(r,k_z,t)=\mathcal{S}_m(k_z)H_m^{(2)}(\Gamma_{0m}r>)J_m(\Gamma_{0m}r<)e^{i(\omega_0+m\Omega)t}, \quad (21)$$

and $S_m\,(k_z)$ is dependent on the type of source. From equations (16) and (19),

$$\text{monopole} \quad \mathcal{S}_m(k_z) = \frac{\pi}{2} Q_0 \rho_0 c_0 (k_{0m} + k_z M), \tag{22}$$

$$\text{dipole} \quad \mathcal{S}_m(k_z) = \frac{\pi}{2} \left(\frac{m}{a} F_{0\phi} + k_z F_{0z}\right). \tag{23}$$

Graf's Addition theorem is now used to transform the incident field to the cylindrical polar coordinate system, $(\bar{r},\ \bar{\phi},\ \bar{z})$, centred on the cylinder. Graf's Addition theorem is given by Abramowitz and Stegun ([12], Eq. 9.1.79, p. 363). The theorem can be used for transforming between the coordinate systems $(r,\ \phi,\ z)$ and $(\bar{r},\ \bar{\phi},\ \bar{z})$ as shown in figure 3. However, the application of Graf's theorem is slightly different depending whether the field point is in the near field (close to the surface of the cylinder) or the far field.

First consider a field point close to the surface of the cylinder where $r > a$ and $\bar{r} < b$[‡]. Direct application of Graf's Addition theorem gives

$$H_m^{(2)}(\Gamma_{0m} r) e^{-im\phi} = (-1)^m e^{-im\beta} \sum_{n=-\infty}^{\infty} H_{m+n}^{(2)}(\Gamma_{0m} b) J_n(\Gamma_{0m} \bar{r}) e^{in(\bar{\phi}-\beta)}. \tag{24}$$

Using this, after some algebraic manipulation, the incident field (21) can be expressed as

$$\overline{p'}_{im}(\bar{r}, k_z, t) = \sum_{n=-\infty}^{\infty} S_n(k_z) e^{i(m-n)\beta} J_n(\Gamma_{0n} a) H_{m-n}^{(2)}(\Gamma_{0n} b) J_m(\Gamma_{0n} \bar{r}) e^{i(\omega_0 + n\Omega)t}. \tag{25}$$

Now consider a field point in the far field where $\bar{r} \gg b$ and $r \gg b$. Direct application of Graf's Addition theorem now gives

$$H_m^{(2)}(\Gamma_{0m} r) e^{-im\phi} = e^{-im\bar{\phi}} \sum_{n=-\infty}^{\infty} H_{m+n}^{(2)}(\Gamma_{0m} \bar{r}) J_n(\Gamma_{0m} b) e^{-in(\bar{\phi}-\beta)}. \tag{26}$$

[‡] It is emphasised that at this point in the analysis, the cylinder has not been included in the modelling. At this stage the aim is to find the incident pressure field at $\bar{r} = a_0$, which will be the location of the surface of the cylinder (when it is included in the subsequent analysis).

Using this, the incident field (21) can be expressed as

$$\overline{p'}_{im}(\bar{r},k_z,t)=\sum_{n=-\infty}^{\infty}\mathcal{S}_n(k_z)e^{im\beta}J_n(\Gamma_{0n}a)H_{m+n}^{(2)}(\Gamma_{0n}\bar{r})J_m(\Gamma_{0n}b)e^{-in\bar{\phi}}e^{i(\omega_0+n\Omega)t}. \tag{27}$$

2.2. Scattered field

Since the scattering object is an infinite cylinder, the scattered acoustic waves will be outward propagating cylindrical waves. An appropriate form of the scattered field p_s' is determined by solving the convected wave equation

$$\frac{\partial^2 p_s'}{\partial\bar{r}^2}+\frac{1}{\bar{r}}\frac{\partial p_s'}{\partial\bar{r}}+\frac{1}{\bar{r}^2}\frac{\partial^2 p_s'}{\partial\bar{\phi}^2}+\frac{\partial^2 p_s'}{\partial\bar{z}^2}-\frac{1}{c_0^2}\left(\frac{\partial}{\partial t}-U\frac{\partial}{\partial\bar{z}}\right)^2 p_s'=0, \tag{28}$$

which is the homogeneous version of equation (3) expressed in the cylinder's polar coordinate system ($\bar{r}$, $\bar{\phi}$, $\bar{z}$).

Following the procedure used to find the incident field, taking the Fourier transform of equation (28) gives equation (10) (Bessel's differential equation) with $\widetilde{p'}_{im}$ replaced by $\widetilde{p'}_{im}$ and r replaced by $\bar{r}$. As $\bar{r}\to\infty$ the solution should decay or represent an outward propagating wave. Applying this radiation condition, it can be shown that the scattered field is given by

$$p_s'(\bar{r},\bar{\phi},\bar{z},t)=\frac{1}{(2\pi)^2}\sum_{m=-\infty}^{\infty}\left(\int_{-\infty}^{\infty}\overline{p'}_{sm}(\bar{r},k_z,t)e^{-ik_z\bar{z}}dk_z\right)e^{-im\bar{\phi}}, \tag{29}$$

where

$$\overline{p'}_{sm}(\bar{r},k_z,t)=\frac{1}{2\pi}\int_{-\infty}^{\infty}C_m(k_z,\omega)H_m^{(2)}(\Gamma\bar{r})e^{i\omega t}d\omega. \tag{30}$$

2.3. Total field

The total pressure field p_t' for a rotating point source located near an infinite, rigid cylinder is given by

$$p_t'=p_i'+p_s' \quad\Rightarrow\quad \overline{p'}_{tm}=\overline{p'}_{im}+\overline{p'}_{sm}. \tag{31}$$

The total field satisfies a rigid wall boundary condition on the surface of the cylinder, i.e.

$$\frac{\partial p_t'}{\partial \bar{r}} = 0 \quad \text{at} \quad \bar{r} = a_0 \quad \Rightarrow \quad \frac{\partial \overline{p'}_{tm}}{\partial \bar{r}} = \frac{\partial \overline{p'}_{im}}{\partial \bar{r}} + \frac{\partial \overline{p'}_{sm}}{\partial \bar{r}} = 0 \quad \text{at} \quad \bar{r} = a_0. \tag{32}$$

On substituting equations (25) and (30) into the boundary condition (32) this leads to

$$\begin{aligned} &\sum_{n=-\infty}^{\infty} S_n(k_z) e^{i(m-n)\beta} J_n(\Gamma_{0n} a) H_{m-n}^{(2)}(\Gamma_{0n} b) \Gamma_{0\boldsymbol{n}} J_m'(\Gamma_{0n} a_0) e^{i(\omega_0 + n\Omega)t} \\ &\quad + \frac{1}{2\pi} \int_{-\infty}^{\infty} C_m(k_z, \omega) \Gamma H_m^{(2)\prime}(\Gamma \boldsymbol{a}_0) e^{i\omega t} d\omega = 0, \end{aligned} \tag{33}$$

where $'$ denotes differentiation with respect to the function's argument.

Equation (33) is solved by first setting

$$C_m(k_z, \omega) = \sum_{n=-\infty}^{\infty} \mathcal{C}_n(m, k_z, \omega) \delta(\omega - [\omega_0 + n\Omega]). \tag{34}$$

Then, substituting C_m (34) into equation (33), and setting each coefficient in the summation equal to zero gives

$$\mathcal{C}_n(m, k_z, \omega_0 + n\Omega) = \frac{-2\pi S_n(k_z) e^{i(m-n)\beta} J_n(\Gamma_{0n} a) H_{m-\boldsymbol{n}}^{(2)}(\Gamma_{0n} b) J_m'(\Gamma_{0n} a_0)}{H_m^{(2)\prime}(\Gamma_{0n} a_0)}. \tag{35}$$

The total pressure field p_t' is given by

$$p_t'(\bar{r}, \bar{\phi}, \bar{z}, t) = \frac{1}{(2\pi)^2} \sum_{m=-\infty}^{\infty} \left(\int_{-\infty}^{\infty} \overline{p'}_{tm}(\bar{r}, k_z, t) e^{-ik_z \bar{z}} dk_z \right) e^{-im\bar{\phi}}. \tag{36}$$

In the near field, close to the surface of the cylinder,

$$\begin{aligned} \overline{p'}_{tm}(\bar{r}, k_z, t) = &\sum_{n=-\infty}^{\infty} \mathcal{S}_n(k_z) e^{i(m-n)\beta} J_n(\Gamma_{0n} a) H_{m-n}^{(2)}(\Gamma_{0n} b) e^{i(\omega_0 + n\Omega)t} \\ &\times \left[\frac{J_m(\Gamma_{0n} \bar{r}) H_m^{(2)\prime}(\Gamma_{0n} a_0) - J_m'(\Gamma_{0\boldsymbol{n}} a_0) H_m^{(2)}(\Gamma_{0n} \bar{r})}{H_m^{(2)\prime}(\Gamma_{0n} a_0)} \right], \end{aligned} \tag{37}$$

where the incident field $\overline{p'}_{im}$ is given by equation (25). In the far field

$$\overline{p'}_{tm}(\bar{r},k_z,t)=\sum_{n=-\infty}^{\infty}S_n(k_z)\,e^{im\beta}J_n(\Gamma_{0n}a)e^{i(\omega_0+n\Omega)t}$$
$$\times\left[\frac{J_m(\Gamma_{0n}b)H^{(2)}_{m+n}(\Gamma_{0n}\bar{r})H^{(2)\prime}_m(\Gamma_{0n}a_0)e^{-in\bar{\phi}}-J'_m(\Gamma_{0n}a_0)H^{(2)}_{m-n}(\Gamma_{0n}b)H^{(2)}_m(\Gamma_{0n}\bar{r})e^{-in\beta}}{H^{(2)\prime}_m(\Gamma_{0n}a_0)}\right], \tag{38}$$

where now the incident field $\overline{p'}_{im}$ is given by equation (27).

Equation (38) is the pressure wavenumber transform in the far field for a rotating, single-frequency, point source located near an infinite, rigid cylinder. In order to calculate the far-field pressure it is necessary to determine the inverse Fourier z-transform, which can be found via an asymptotic evaluation of the integral, using the method of stationary phase. The presence of a uniform mean flow complicates the stationary phase integral, but this complication can be removed by using flow similarity variables and a transformation of the axial wavenumber.

The far-field pressure will be expressed in the spherical polar coordinates ($\bar{R}$, $\bar{\theta}$, $\bar{\phi}$), where

$$\bar{r}=\bar{R}\sin\bar{\theta}\quad\text{and}\quad\bar{z}=\bar{R}\cos\bar{\theta}. \tag{39}$$

Then, following Chapman [13], the similarity variables $\hat{R}$ and $\hat{\theta}$ are introduced. These are related to $\bar{R}$ and $\bar{\theta}$ by

$$\hat{R}=\frac{\bar{R}}{\sigma}(1-M^2\sin^2\bar{\theta})^{\frac{1}{2}},\quad\cos\hat{\theta}=\frac{\cos\bar{\theta}}{(1-M^2\sin^2\bar{\theta})^{\frac{1}{2}}}$$
$$\text{and}\quad\sin\hat{\theta}=\frac{\sigma\sin\bar{\theta}}{(1-M^2\sin^2\bar{\theta})^{\frac{1}{2}}}, \tag{40}$$

where $\sigma^2=1-M^2$. (Also note that $\bar{R}\sin\bar{\theta}=\hat{R}\sin\hat{\theta}$ and $\bar{R}\cos\bar{\theta}=\hat{R}\,\sigma\cos\hat{\theta}$.)

The inverse Fourier z-transform in equation (36) can be expressed in the form of a stationary phase integral, replacing $H^{(2)}_{m+n}(\Gamma_{0n}\bar{r})$ and $H^{(2)}_m(\Gamma_{0n}\bar{r})$ by their large-argument asymptotic forms, and by using Chapman's similarity variables. Also, following Rienstra [14], the axial wavenumber k_z is transformed, via

$$\tau=\sigma^2\frac{k_z}{k_{0n}}-M, \tag{41}$$

so that τ is now the integration variable. After some algebraic manipulation, it can be shown that

$$k_z = \frac{k_{0n}}{\sigma^2}(\tau + M) \quad \text{and} \quad \Gamma_{0n} = \frac{k_{0n}}{\sigma}(1-\tau^2)^{\frac{1}{2}}. \tag{42}$$

After these changes of variables, the point of stationary phase is found to be $\tau = \cos\hat{\theta}$, and it is more straightforward to evaluate the stationary phase integral. This leads to, in the far field $\bar{R} \gg 1$, the total pressure

$$p_t'(\bar{R},\bar{\theta},\bar{\phi},t) \sim \frac{i}{4\pi\bar{R}} \frac{1}{(1-M^2\sin^2\bar{\theta})^{1/2}} \sum_{m=-\infty}^{\infty}\sum_{n=-\infty}^{\infty} \frac{2\mathcal{S}_n}{\pi} e^{-ik_{0n}\bar{R}S(\bar{\theta})} e^{i(\omega_0+n\Omega)t} e^{im(\beta+\pi/2)} e^{-im\bar{\phi}} \times \left[\frac{J_n(\Delta_n a)J_m(\Delta_n b)H_m^{(2)\prime}(\Delta_n a_0)e^{-in(\bar{\phi}-\pi/2)} - J_n(\Delta_n a)J_m'(\Delta_n a_0)H_{m-n}^{(2)}(\Delta_n b)e^{-in\beta}}{H_m^{(2)\prime}(\Delta_n a_0)}\right], \tag{43}$$

where

$$\Delta_n = \frac{k_{0n}\sin\bar{\theta}}{(1-M^2\sin^2\bar{\theta})^{1/2}}. \tag{44}$$

In the far-field, the source term becomes

$$\text{monopole} \quad \frac{2\mathcal{S}_n}{\pi} \to \frac{Q_0\rho_0 c_0 k_{0n} S(\bar{\theta})}{(1-M^2\sin^2\bar{\theta})^{1/2}}, \tag{45}$$

$$\text{dipole} \quad \frac{2\mathcal{S}_n}{\pi} \to \left(\frac{n}{a}F_{0\phi} + \frac{k_{0n}}{(1-M^2\sin^2\bar{\theta})^{1/2}}T(\bar{\theta})F_{0z}\right). \tag{46}$$

Also, $S(\bar{\theta})$[§] and $T(\bar{\theta})$ are defined as

$$S(\bar{\theta}) = \frac{\left((1-M^2\sin^2\bar{\theta})^{1/2} + M\cos\bar{\theta}\right)}{(1-M^2)} \quad \text{and} \quad T(\bar{\theta}) = \frac{\left(M(1-M^2\sin^2\bar{\theta})^{1/2} + \cos\bar{\theta}\right)}{(1-M^2)}. \tag{47}$$

[§]Note that in other articles the definition of $S(\bar{\theta})$ may vary slightly, specifically the sign of M. In this analysis, in the moving frame of reference the uniform flow is $-U$ in the positive $\bar{z}$-direction. This accounts for the different sign of M which is taken here.

2.4. Solution for a rotating ring of point sources

Equation (43) gives the far-field pressure due to a rotating point source. This could be used to model the radiation from a single rotor blade. Hanson ([15], Appendix: Effect of Multiple Blades, p. 617) outlines how to extend a radiation model for one blade to multiple blades. His approach is followed here, for an example based on a 'rotor-rotor' interaction tone generated by a contra-rotating propeller.

An illustration of the problem set-up is shown in figure 4. The rotors are labelled 1 and 2. Rotor 1 is modelled by a distribution of identical point sources, equi-spaced around a circle of radius a. Denote the total number of sources by B (which equals the number of rotor blades of rotor 1), and number the sources $p = 0, 1, 2, \ldots, B - 1$. The angular velocity of rotor 1 $\dot{\phi} = \Omega$. Rotor 2 is also represented by a distribution of identical point sources, equi-spaced around a circle of radius a_k. Denote the total number of sources by B_k (which equals the number of rotor blades of rotor 2). The angular velocity of rotor 2 $\dot{\phi} = -\Omega_k$. Only a single reference blade (i.e. point source) from rotor 2 is shown. In the sketch, when sources from rotor 1 and rotor 2 are aligned (in a vertical sense) this signifies an 'interaction' between the two blades, for example, owing to the wake or potential field from one rotor blade interacting with a blade on the other rotor.

It is convenient to view the problem in the reference frame of rotor 1. In this reference frame, the moving angular coordinate $\tilde{\phi} = \phi - \Omega t$, and the angular velocity of rotor 2 is $-(\Omega + \Omega_k)$. Taking the incident field due to point source $p = 0$ given by equations (20, 21), then the incident field due to source p will be essentially the same, apart from it is necessary to apply an angular correction and a time shift. The angular correction is

$$\tilde{\phi} \to \tilde{\phi} - \frac{2\pi p}{B}. \tag{48}$$

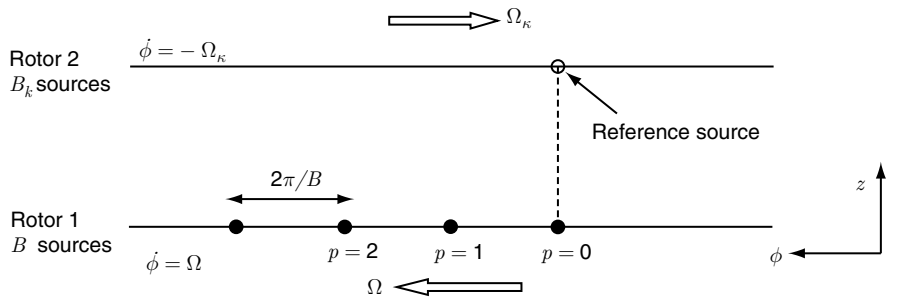

Figure 4: Illustration showing set-up for modelling rotor-rotor interaction tones.

Assuming that point source $p = 0$ coincides with the reference source at $t = 0$, then source p coincided with the reference source at time $t = -2\pi p/B\,(\Omega + \Omega_k)$. Therefore, the time shift is

$$t \to t + \frac{2\pi p}{B(\Omega + \Omega_k)}. \tag{49}$$

Then, the total incident field is given by

$$p_i'(r, \phi, z, t) = \sum_{p=0}^{B-1} p_i'^{(p)}, \tag{50}$$

where $p_i'^{(p)}$ denotes the incident field due to point source p.

In equation (50), the summation over p can be evaluated using the standard formula for a geometric progression. The resulting incident field due to a rotating ring of point sources is of the same form as the field due to a single, rotating point source, given by equations (20, 21), apart from an additional multiplicative factor B, and the summation index is replaced by l, where $m = lB - kB_k$. Also, the source frequency is given by $\omega_0 = kB_k\,(\Omega + \Omega_k)$ which represents the kth harmonic of unsteady loading.

Then, in order to determine the total pressure field in the presence of an infinite, rigid cylinder, the analysis follows the same procedure as before. In the far field, $\bar{R} \gg 1$, the total pressure

$$\begin{aligned} p_t'(\bar{R}, \bar{\theta}, \bar{\phi}, t) \sim \frac{iB}{4\pi\bar{R}} \frac{1}{(1 - M^2 \sin^2\bar{\theta})^{1/2}} \sum_{m=-\infty}^{\infty} \sum_{l=-\infty}^{\infty} \frac{2S_n}{\pi} e^{-ik_{0_n}\bar{R}S(\bar{\theta})} e^{i(\omega_0 + n\Omega)t} e^{im(\beta + \pi/2)} e^{-im\bar{\phi}} \\ \times \left[\frac{J_n(\Delta_n a) J_m(\Delta_n b) H_m^{(2)\prime}(\Delta_n a_0) e^{-in(\bar{\phi} - \pi/2)} - J_n(\Delta_n a) J_m'(\Delta_n a_0) H_{m-n}^{(2)}(\Delta_n b) e^{-in\beta}}{H_m^{(2)\prime}(\Delta_n a_0)} \right], \end{aligned} \tag{51}$$

where $n = lB - kB_k$. Note that it would be necessary to include a third summation over k in equation (51) in order to include all the harmonics of unsteady loading (see section 3.2). If the loading is due to interaction with a pylon wake, or something else which is analogous to 'rotor-stator' interaction tones in a turbofan engine, then set $\Omega_k = 0$. Equation (51) is also applicable for rotor-alone tones, on setting $B_k = 0$, and so $n = lB$ and $\omega_0 = 0$.

2.5. Illustrative results

A selection of illustrative results are shown in this section. One rotating ring of steady monopole sources is considered (so $B_k = 0$ and $\omega_0 = 0$). The number of sources $B = 12$, the radius of the cylinder $a_0 = 2$ m, and the axial Mach number $M = 0.7$. The values of the other parameters (b, β, a and Ω) are listed in the figure captions¶.

¶The values of c_0 and ρ_0 are based on the values for the standard atmosphere at 30, 000 ft.

The far-field mean square pressure azimuthal directivity (in dB), at polar angle $\bar{\theta} = 90°$, are shown for several different test cases. In these examples, taking $\omega_0 = 0$, the evaluation of the mean square pressure from $p'_t(\bar{R}, \bar{\theta}, \bar{\phi}, t)$ (51) is straightforward. Also shown are the comparable far-field directivity patterns when there is no cylinder.

Figures 5 and 6 show how changing the source rotation direction (sign of Ω), or the orientation of the ring of sources relative to the cylinder (angle β), affects the far-field

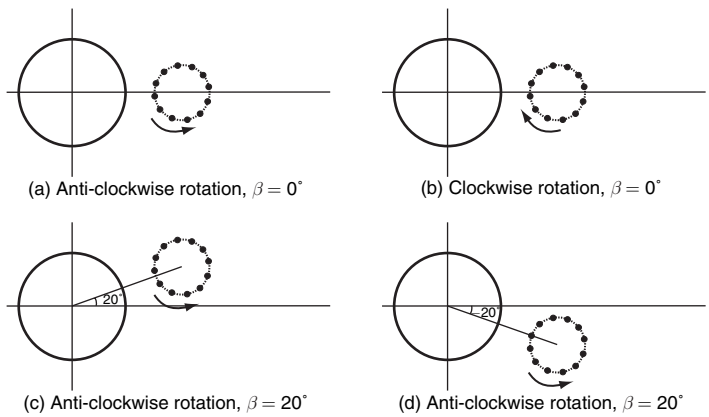

Figure 5: Installed open rotor configuration. $B = 12$, $a_0 = 2$ m, $a = 1$ m, $b - a_0 - a = 1$ m, $\Omega a/c_0 = 0.5$ and $M = 0.7$.

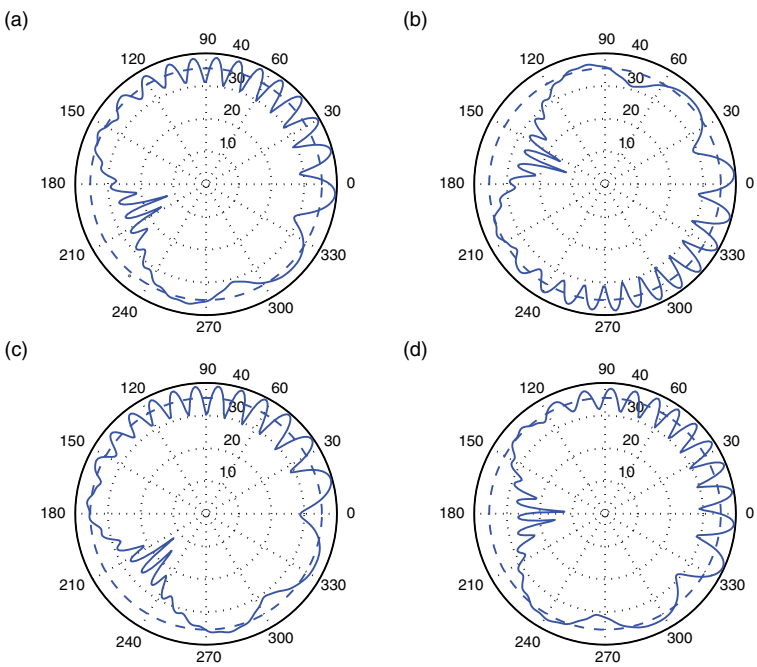

Figure 6: Far-field mean square pressure azimuthal directivity (in dB) at polar angle $\bar{\theta} = 90°$. Key: solid line, with cylinder; dashed line, no cylinder.

mean square pressure azimuthal directivity. In each case, as expected, only the orientation of the directivity pattern is altered. The directivity pattern is the mirror image, reflected about the horizontal plane, when the sources' rotation direction is reversed. Changing the angle β simply moves the directivity pattern through the same angular shift.

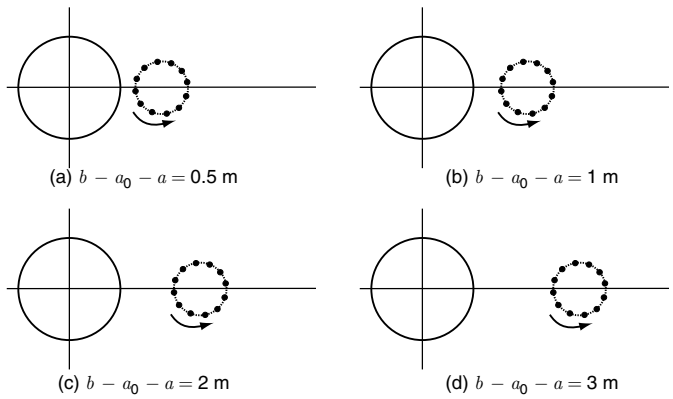

Figure 7: Installed open rotor configuration. Anti-clockwise rotation. $B = 12$, $a_0 = 2$ m, $a = 1$ m, $\beta = 0°$, $\Omega a/c_0 = 0.5$ and $M = 0.7$.

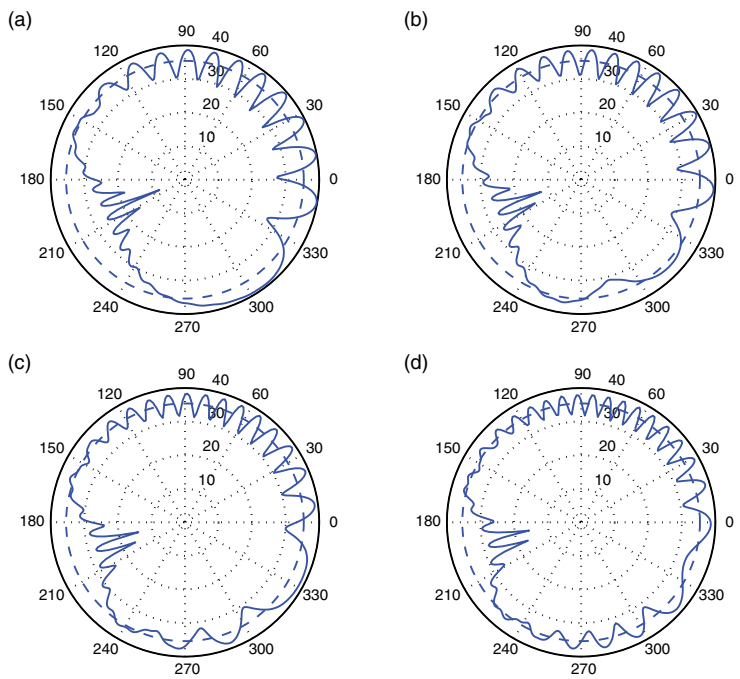

Figure 8: Far-field mean square pressure azimuthal directivity (in dB) at polar angle $\bar{\theta} = 90°$. Key: solid line, with cylinder; dashed line, no cylinder.

Figures 7 and 8 show how changing the distance between the ring of sources and the cylinder affects the far-field directivity. The main effect owing to the presence of the cylinder, other than the expected 'lobed' directivity pattern, is that at some azimuthal angles the level of the mean square pressure is significantly lower compared to the level with no cylinder. For example, in figure 8(a), lower mean square pressure levels are predicted in the azimuthal angular range from $\bar{\phi} = 160°$ to $260°$. As the ring of sources is moved away from the cylinder, the extent of these regions of lower mean square pressure become smaller.

The minimum level of the mean square pressure does not occur at $\bar{\phi} = 180°$. This is because the source is rotating. The minimum level of the mean square pressure, in these cases, occurs at a value of $\bar{\phi}$ slightly greater than $180°$. At the azimuthal angles where the predicted mean square pressure is significantly lower compared to the level with no cylinder, the source will be moving away from an observer at these locations. Presumably this effect is related to convective amplification which occurs with moving sources.

Finally, Figures 9 and 10 also show the effect of changing the distance between the ring of sources and the cylinder, but now the source radius and the cylinder radius are the same.

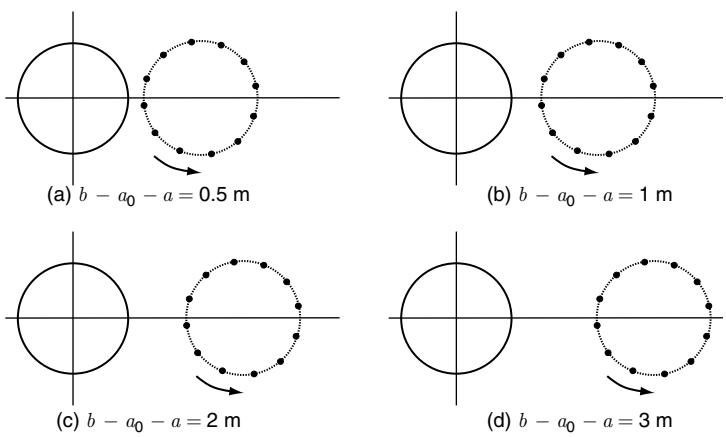

Figure 9: Installed open rotor configuration. Anti-clockwise rotation. $B = 12$, $a_0 = 2$ m, $a = 2$ m, $\beta = 0°$, $\Omega a/c_0 = 0.5$ and $M = 0.7$.

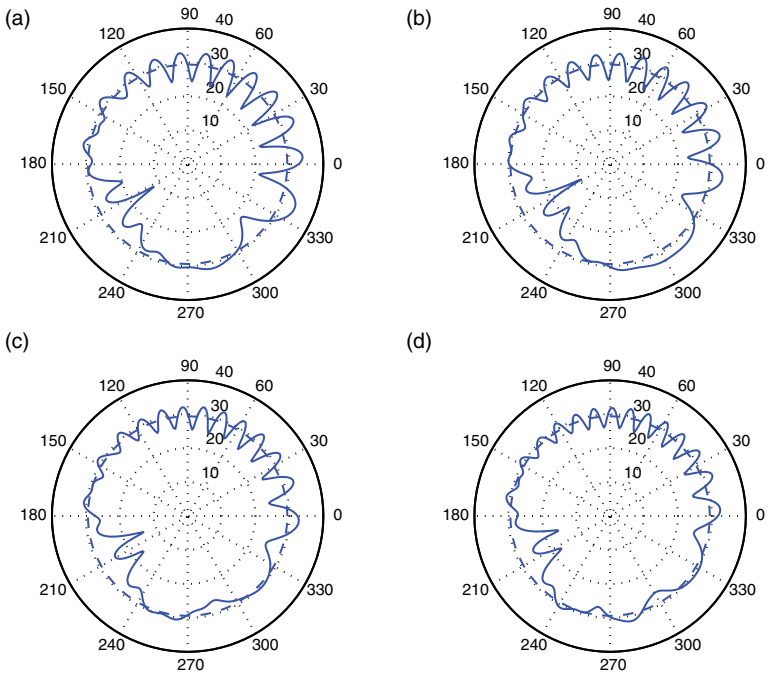

Figure 10: Far-field mean square pressure azimuthal directivity (in dB) at polar angle $\bar{\theta} = 90°$. Key: solid line, with cylinder; dashed line, no cylinder.

Reductions in the level of the mean square pressure, due to presence of the cylinder, still occur, but the shielding effect is less in these test cases when the source and cylinder radii are comparable.

3. DISTRIBUTED SOURCE MODEL

In propeller noise theory it is common (see for example Refs. [8, 15, 16]) to express the pressure in terms of 'emission' coordinates. The emission coordinate system is shown in figure 11.

The emission coordinate system is related to the physical coordinate system in Cartesian and spherical coordinates by the following relationships:

$$\bar{x}_e = \bar{x}, \quad \bar{y}_e = \bar{y}, \quad \bar{z}_e = \left(\bar{z} + M\sqrt{\bar{z}^2 + \sigma^2(\bar{x}^2 + \bar{y}^2)}\right) / \sigma^2; \tag{52}$$

$$\begin{aligned} &\bar{x}_e = \bar{R}_e \sin\bar{\theta}_e \cos\bar{\phi}_e, \quad \bar{y}_e = \bar{R}_e \sin\bar{\theta}_e \sin\bar{\phi}_e, \\ &\bar{z}_e = \bar{R}_e \cos\bar{\theta}_e, \quad \bar{R}_e = \sqrt{\bar{x}_e^2 + \bar{y}_e^2 + \bar{z}_e^2}. \end{aligned} \tag{53}$$

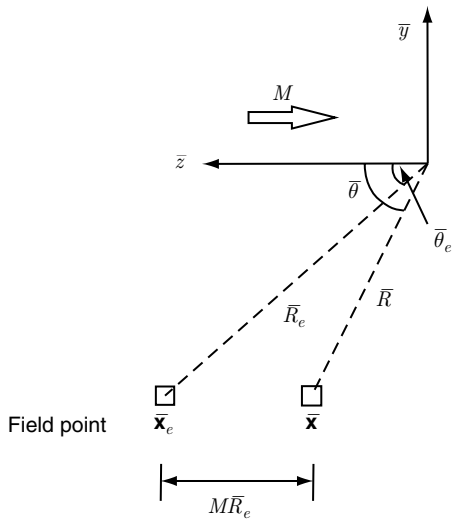

Figure 11: Observer coordinates: physical and 'emission' coordinate systems.

The emission coordinate system is employed in the following analysis which details the far-field pressure for both thickness and loading noise based on a distributed source model which simulates the noise sources generated by an open rotor.

3.1. Thickness noise

When expressed in emission coordinates, equation (51) for a rotating ring of steady monopole sources† at arbitrary source radius r, adjacent to an infinite, rigid cylinder and immersed in a constant axial flow of Mach number M in the negative axial direction, becomes

$$
\begin{aligned}
p_t'(\bar{R}_e,\bar{\theta}_e,\bar{\phi}_e,t) \sim{}& \frac{iB}{4\pi\bar{R}_e}\frac{1}{(1-M\cos\bar{\theta}_e)}\\
&\sum_{m=-\infty}^{\infty}\sum_{l=-\infty}^{\infty}\left(\frac{Q_0\rho_0c_0k_{0n}}{(1-M\cos^2\bar{\theta}_e)}\right)e^{i(n\Omega t-k_{0n}\bar{R}_e)}e^{im(\beta+\pi/2)}e^{-im\bar{\phi}}\\
&\times\left[\frac{J_n(\Delta_n r)J_m(\Delta_n b)H_m^{(2)\prime}(\Delta_n a_0)e^{-in(\bar{\phi}_e-\pi/2)}-J_n(\Delta_n r)J_m'(\Delta_n a_0)H_{m-n}^{(2)}(\Delta_n b)e^{-in\beta}}{H_m^{(2)\prime}(\Delta_n a_0)}\right],
\end{aligned}
\tag{54}
$$

†In this case the monopole source term is given by (45).

where $n = lB$, $k_{0n} = n\Omega/c_0$ and

$$\Delta_n = \frac{k_{0n}\sin\bar{\theta}_e}{(1-M\cos\bar{\theta}_e)}. \tag{55}$$

The effect of sweep and chordwise position of a source located on the blade planform also needs to be taken into account. The local blade geometry is shown in figure 12.

From inspection of figure 12, a point source located at radius r and chordwise location X is offset from the pitch-change axis in the axial direction by a distance $-(s + X)\cos\alpha$, where s and α are the blade sweep‡ and stagger angle, which are both functions of the spanwise location. The effect of the axial offset can be included by replacing $\bar{z}$ in equation (36) by $\bar{z} + (s + X)\cos\alpha$. This introduces a multiplicative factor $\exp\{-ik_z(s + X)\cos\alpha\}$ in the Fourier integral in equation (36). On evaluating this integral, using the method of stationary phase, the stationary phase point occurs at

$$k_z = \frac{k_{0n}\cos\bar{\theta}_e}{(1-M\cos\bar{\theta}_e)}. \tag{56}$$

Thus the axial offset introduces the following multiplicative factor into equation (54):

$$\exp\left\{-i\frac{k_{0n}\cos\bar{\theta}_e}{(1-M\cos\bar{\theta}_e)}(s+X)\cos\alpha\right\}. \tag{57}$$

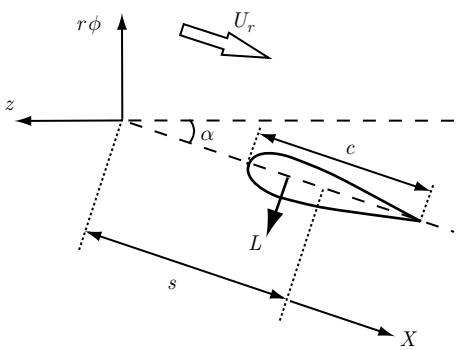

Figure 12: Local rotor-blade geometry.

‡ Note that sweep is measured as the distance of the blade mid-chord to the pitch-change axis along the helical path as shown in figure 12.

The source is also offset in the azimuthal direction ϕ by an angle $-(s + X) \sin \alpha /r$. The effect of the tangential offset is to introduce an angular correction and a time shift to the expression for the total field (54). The process for calculating this correction is identical to that described in section 2.4. Including the source tangential offset in the analysis introduces an additional multiplicative factor into equation (54):

$$\exp\left\{-i\frac{n}{r}(s+X)\sin\alpha\right\}. \tag{58}$$

In reality, the monopole sources are distributed over the upper and lower blade surfaces. However, it is an acceptable approximation to instead place the monopole sources associated with both the upper and lower blade surfaces along the chordline. Thus for the thickness noise prediction, each rotor blade is modeled as being acoustically equivalent to a distribution of monopole sources over the blade planform area[§]. The thickness noise distributed source strength is equal to the net rate of volume displacement produced by each blade. The net rate of volume displacement produced by an element of area $\delta X \delta r$ is given by

$$Q_0 = U_r b \frac{dh}{dX} \delta X \delta r, \tag{59}$$

where $U_r = \sqrt{U^2 + (r\Omega)^2}$ is the local blade helical speed (i.e. the relative velocity seen by an observer on the rotor blade at radius r), b is the maximum blade thickness, and h is a dimensionless function, which has a maximum value of one, and which describes the chordwise blade thickness profile. Substituting equation (59) into equation (54), multiplying by equations (57) and (58), and integrating over the blade planform area yields the following expression for the far-field sound pressure produced by an open rotor located adjacent to an infinite, rigid cylindrical fuselage:

$$\begin{aligned} p_t'(\bar{R}_e, \bar{\theta}_e, \bar{\phi}_e, t) \sim{}& \frac{-B}{4\pi\bar{R}_e} \frac{1}{(1 - M\cos\bar{\theta}_e)} \\ & \sum_{m=-\infty}^{\infty} \sum_{l=-\infty}^{\infty} \left(\frac{\rho_0 c_0 k_{0n}}{(1 - M\cos^2\bar{\theta}_e)} \right) \int_{rh}^{rt} U_r b J_n(\Delta_n r) \Psi_V k X e^{-i\phi_s} dr \\ & \times e^{i(n\Omega t - k_{0n}\bar{R}_e)} e^{im(\beta+\pi/2)} e^{-im\bar{\phi}_e} \left[J_m(\Delta_n b) e^{-in(\bar{\phi}_e - \pi/2)} - \frac{J_m'(\Delta_n a_0)}{H_m^{(2)\prime}(\Delta_n a_0)} H_{m-n}^{(2)}(\Delta_n b) e^{-in\beta} \right], \end{aligned} \tag{60}$$

[§]Here the blade planform area is defined as the surface formed by the chordlines across the blade span.

where

$$\Psi_V = \int_{-1/2}^{1/2} h(\tilde{X}) e^{-ik_x \tilde{X}} d\tilde{X}, \quad (\tilde{X} = X/c) \tag{61}$$

is a non-compactness factor which accounts for the difference in phase of sources distributed along the blade chord,

$$k_X = \left(\frac{n}{r} \sin\alpha + \frac{k_{0n} \cos\overline{\theta}_e}{(1 - M\cos\overline{\theta}_e)} \cos\alpha \right) c \tag{62}$$

is a chordwise wavenumber, and

$$\phi_s = \left(\frac{n}{r} \sin\alpha + \frac{k_{0n} \cos\overline{\theta}_e}{(1 - M\cos\overline{\theta}_e)} \cos\alpha \right) s \tag{63}$$

is a phase term which accounts for the effect of sweep.

3.2. Loading noise

The procedure for deriving the expression for the far-field pressure produced by loading on the rotor blades is similar to that presented in the previous section for thickness sources. Each rotor blade is modeled as being acoustically equivalent to a distribution of dipoles over the blade planform area. The dipole source strength at a particular location is equal to the net loading exerted by the rotor blade on the surrounding air which is equal to the pressure 'jump' or difference in pressure between the upper and lower blade surfaces. It is assumed that only lift forces are significant and thus the loading is modeled as acting normal to the blade chordline. From inspection of figure 12, the axial component of loading is $F_{0z} = -L \sin\alpha$, while the azimuthal component of loading is $F_{0\phi} = L \cos\alpha$.

The unsteady loading on the rotor blades is assumed to be caused by a counter-rotating disturbance with azimuthal periodicity of $2\pi/B_k$ radians which rotates at an angular speed $\dot{\phi} = -\Omega_k$. The loading exerted by each rotor blade on the air in a frame of reference moving with the rotor blade can thus be expressed as a Fourier series

$$L(r, X, t) = \sum_{k=-\infty}^{\infty} L_k(r, X) e^{i\omega_0 t}, \tag{64}$$

where $\omega_0 = kB_k(\Omega + \Omega_k)$.

The far-field pressure produced by a rotating ring of point forces, with axial component F_{0z}, and tangential component $F_{0\phi}$, adjacent to an infinite, rigid cylinder and immersed in a constant axial flow of Mach number M in the negative axial direction, is

given by equation (51) with the dipole source term given by (46). Inserting equation (64) into equation (51) and substituting expressions for the axial and tangential loading gives

$$
\begin{aligned}
&p_t'(\bar{R},\bar{\theta},\bar{\phi},t) \sim \frac{-iB}{4\pi\bar{R}} \frac{1}{(1-M^2\sin^2\bar{\theta})^{1/2}} \sum_{m=-\infty}^{\infty} \sum_{l=-\infty}^{\infty} \sum_{k=-\infty}^{\infty} \\
&L_k\left(-\frac{n}{r}\cos\alpha + \frac{k_{0n}}{(1-M^2\sin^2\bar{\theta})^{1/2}} T(\bar{\theta})\sin\alpha\right) \times e^{-ik_{0n}\bar{R}S(\bar{\theta})} e^{i(\omega_0+n\Omega)t} e^{im(\beta+\pi/2)} e^{-im\bar{\phi}} \\
&\times\left[\frac{J_n(\Delta_n r)J_m(\Delta_n b)H_m^{(2)'}(\Delta_n a_0)e^{-in(\bar{\phi}-\pi/2)} - J_n(\Delta_n r)J_m'(\Delta_n a_0)H_{m-n}^{(2)}(\Delta_n b)e^{-in\beta}}{H_m^{(2)'}(\Delta_n a_0)}\right],
\end{aligned}
\tag{65}
$$

where $n = lB - kB_k$ is an azimuthal wavenumber. Note that the angular frequency can be rewritten as

$$
\begin{aligned}
\omega_0 + n\Omega &= kB_k(\Omega + \Omega_k) + (lB - kB_k)\Omega \\
&= lB\Omega + kB_k\Omega_k,
\end{aligned}
\tag{66}
$$

i.e. in terms of sum and difference tones. Thus, it is convenient to introduce a slight change in notation as follows:

$$\omega_{lk} = lB\Omega + kB_k\Omega_k, \tag{67}$$

$$k_{lk} = \omega_{lk} / c_0, \tag{68}$$

$$\text{and} \qquad \Delta_{lk} = \frac{k_{lk}\sin\bar{\theta}}{(1-M^2\sin^2\bar{\theta})^{1/2}}. \tag{69}$$

Following this notation change, this means that in equation (65), $\omega_0 + n\Omega$ may be replaced by ω_{lk}, k_{0n} may be replaced by k_{lk}, and Δ_n may be replaced by Δ_{lk}.

Converting to emission coordinates, accounting for the axial and tangential offset produced by the sources located along the blade chord¶, and integrating over the blade planform area yields the following expression for the far-field sound pressure due to periodic unsteady loading on the blades of an open rotor located adjacent to an infinite, rigid cylindrical fuselage:

¶Note that in the case of unsteady blade loading, the axial and tangential offset of a source located at chordwise position X on a swept blade introduces a multiplicative factor of $\exp\{-\mathrm{i}\,(k_{lk}\cos\bar{\theta}_e/(1 - M\cos\bar{\theta}_e) + (n/r)\sin\alpha)\,(s + X)\}$

$$p'_t(\bar{R}_e,\bar{\theta}_e,\bar{\phi}_e,t) \sim \frac{-iB}{4\pi\bar{R}_e}\frac{1}{(1-M\cos\bar{\theta}_e)}$$
$$\sum_{m=-\infty}^{\infty}\sum_{l=-\infty}^{\infty}\sum_{k=-\infty}^{\infty}\int_{r_h}^{r_t} S(r)J_n(\Delta_{lk}r)e^{-i\phi_s}dr$$
$$\times e^{i(\omega_{lk}t-k_{lk}\bar{R}_e)}e^{im(\beta+\pi/2)}e^{-im\bar{\phi}_e}\left[J_m(\Delta_{lk}b)e^{-in(\bar{\phi}_e-\pi/2)} - \frac{J'_m(\Delta_{lk}a_0)}{H^{(2)'}_m(\Delta_{lk}a_0)}H^{(2)}_{m-n}(\Delta_{lk}b)e^{-in\beta}\right], \quad (70)$$

where the function $S(r)$ is given by

$$S(r) = \left(-\frac{n}{r}\cos\alpha + \frac{k_{lk}\cos\bar{\theta}_e}{(1-M\cos\bar{\theta}_e)}\sin\alpha\right)\Psi_L, \quad (71)$$

and

$$\Psi_L = c\int_{-1/2}^{1/2} L_k(r,\tilde{X})e^{-ik_X\tilde{X}}d\tilde{X}, \quad (\tilde{X} = X/c). \quad (72)$$

The chordwise wavenumber k_X and phase term ϕ_s are given by equations (62) and (63) respectively, with k_{0n} replaced by k_{lk}.

3.3. Illustrative results

In this section, additional illustrative results are presented which provide more practically relevant examples of noise predictions for an installed open rotor. The effect of fuselage scattering on the sound field produced by two different force distributions is considered. The first corresponds to a rotating point force, acting in the negative axial direction and located at $r = a$, for which the amplitude varies as a function of blade azimuthal position $\phi = \Omega t$ (for the reference blade) given by

$$F_{0z} = \delta(X)\frac{\delta(r-a)}{r}\frac{L_0}{1+(\phi/\phi_s)^2}, \quad (73)$$

where L_0 is an amplitude term, and $\phi_s = 3.75°$[‖]. This loading is 'impulsive', having large amplitude as the blade passes through $\phi = 0°$ and small amplitude elsewhere, and could be thought of as being similar to the loading produced when a blade passes

[‖]This loading function was first considered by Glegg [7] who used it to investigate scattering from a propeller centerbody.

through the wake of an upstream pylon. In this scenario the pylon (at $\phi = 0°$) would be vertically aligned, which is representative of a rotor hung beneath a wing. As the loading is not distributed over the blade chord and span, the sound field can be evaluated very rapidly. Also, effects such as interference from sources located at different chordwise and radial locations are not included. It has been found by the authors that, because of these simplifications, this function is useful for investigating the characteristics of the scattered sound field.

Figures 13 and 14 plot sound pressure time histories produced by one propeller blade with a source Mach number $\Omega a/c_0 = 0.7$. The fuselage radius is $a_0 = 2a$ and the fuselage axis is located at $b = 4a$ and $\beta = 270°$ (figure 13) or $\beta = 90°$ (figure 14) relative to the propeller axis. The location of the impulsive force on the rotor blades is indicated by two concentric red circles located at $r = a$, $\phi = 0°$. This corresponds to a propeller mounted adjacent to the fuselage with a pylon located at $\phi = 0°$ and is representative of a case where the propeller was mounted either directly above or below the wing.

For both cases, four far-field observation points are considered at azimuthal angles $\bar{\phi} = 0°$, $90°$, $180°$ and $270°$. Each observation point is located at polar emission angle $\bar{\theta}_e = 45°$. The incident (free) field sound pressure time history is shown in black, while the red curve corresponds to the total pressure which is the sum of the incident and scattered fields. The incident field (black) curve has been superimposed upon the total field curve (red).

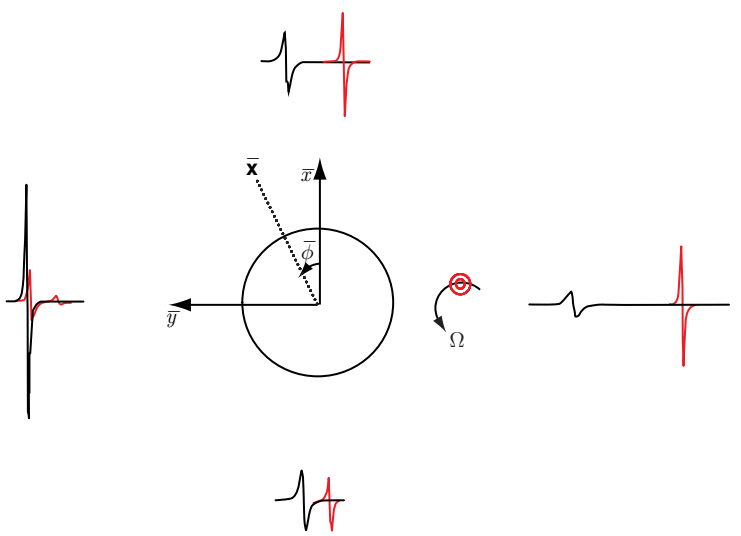

Figure 13: Sound pressure time histories, due to an impulsive source on a propeller located at $\beta = 270°$. Key: black line, incident (free-field) pressure; red line, total pressure.

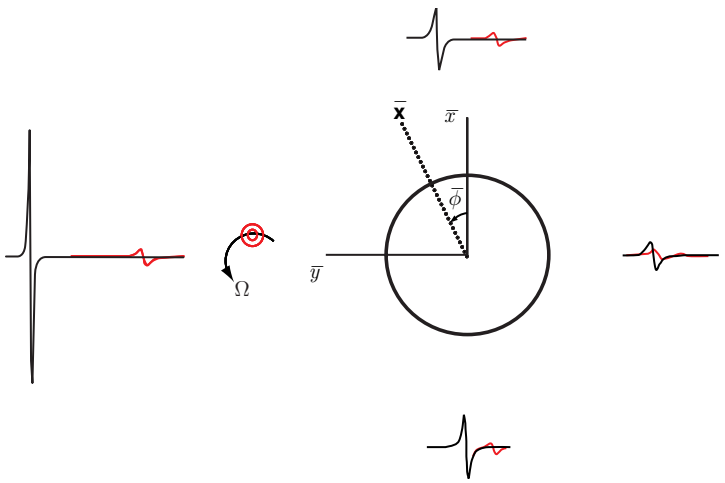

Figure 14: Sound pressure time histories, for the case shown in figure 13 but with $\beta = 90°$.

Inspection of figures 13 and 14 shows that the free-field pulse generated by the propeller blade has maximum amplitude at $\bar{\phi} = 90°$ and minimum amplitude at $\bar{\phi} = 270°$. This is presumably due to convective amplification effects. When the blade passes through the point of maximum loading at $\phi = 0°$, a relatively significant level of sound is generated. At this point the blade is moving towards the observer at $\bar{\phi} = 90°$. As is observed, this increases the amplitude of the pressure pulse relative to an observer located at $\bar{\phi} = 0°$ or $\bar{\phi} = 180°$ for which the blade is neither moving towards nor away from the observer, (see for example chapter 1 of Goldstein [17]). Conversely, for an observer located at $\bar{\phi} = 270°$ the blade is moving away from the observer, which decreases the amplitude of the pressure pulse.

From a practical point of view this means that for the case considered here, if the propeller is located on the negative $\bar{y}$-axis then the sound pressure incident on the fuselage is of relatively large amplitude. This results in a reflected acoustic pulse of significant amplitude at all angles. It is interesting to note that the reflected pulses at $\bar{\phi} = 0°$ and $\bar{\phi} = 270°$ have significantly larger amplitudes than the incident field pulses at these angles. Conversely, if the propeller is located on the positive $\bar{y}$-axis then the sound pressure incident on the fuselage is of relatively small amplitude and consequently the reflected acoustic pulses have amplitudes, which relative to the propeller on the negative $\bar{y}$-axis, are significantly smaller.

Thus it can be deduced that for impulsive loading, such as occurs when a rotor blade passes through a pylon wake, the sound which is generated radiates primarily in the direction that the blade is moving at the time when the impulsive loading occurs. Thus by either placing an upstream pylon in an appropriate position, or by ensuring that the propeller rotates in a direction such that it is moving away from the fuselage when it

passes through the pylon wake, the sound radiated towards the fuselage will be minimized. This will minimize both the in-cabin noise and also the level of the scattered field.

The second case considered here corresponds to the loading induced on a propeller due to its interaction with the viscous wake of an upstream pylon. The pylon wake velocity deficit is modeled using the Gaussian wake described in Parry [18]. As the solidity of an open rotor is relatively low, the 'blade response', or unsteady loading due to the interaction of the rotor blades with the pylon wake was calculated using isolated aerofoil theory (cf. Parry [16]). The free-stream and blade tip Mach numbers are, respectively, 0.2 and 0.7. The rotor blade chord and sweep distributions are identical to the blade described in Whitfield *et al.* [3]. Otherwise, the parameters used in the previous case remain the same, albeit $a_0 = 2r_t$ and $b = 4r_t$.

The mean square pressure azimuthal directivity pattern of the first two interaction tones are shown respectively in figures 15 and 16. Unlike the time-domain simulation, the effect of source motion (i.e. convective amplification) on the azimuthal directivity is not immediately apparent. However, the effect of the fuselage on the scattered field is clearly observed. At angles for which the fuselage obscures the observer position, a significant reduction in sound pressure level occurs.

The effect of pylon length on the radiated sound field is now briefly investigated. In figure 17 again the azimuthal directivity of the first interaction tone is plotted at polar angle $\bar{\theta} = 45°$. The propeller is located at $\beta = 270°$ while the pylon is vertically aligned, i.e. located at $\phi = 0°$. Both the propeller and section of the pylon for which the wake impinges on the rotor disc are identical to those considered in figures 15 and 16. The distance between the rotor and the cylindrical fuselage is varied from $b = 3.5r_t$

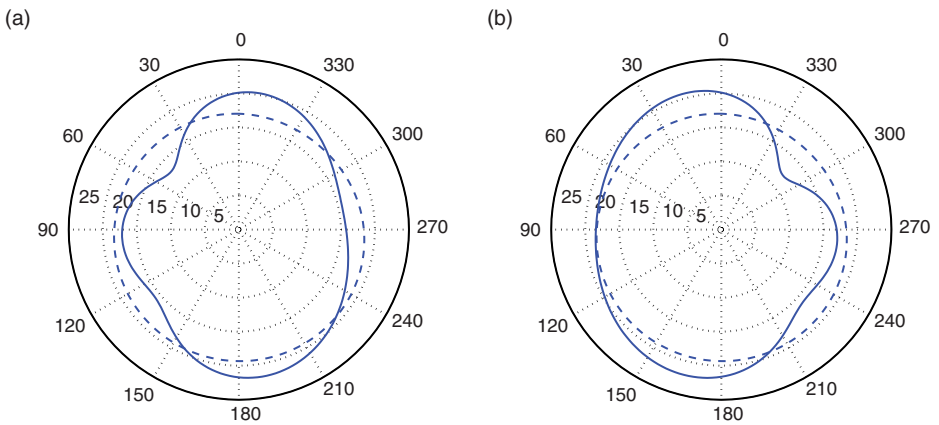

Figure 15: Far-field mean square pressure azimuthal directivity (in dB) of the first interaction tone at polar angle $\bar{\theta} = 45°$. The propeller is located at: (a) $\beta = 270°$; (b) $\beta = 90°$. Key: solid line, with cylinder; dashed line, no cylinder.

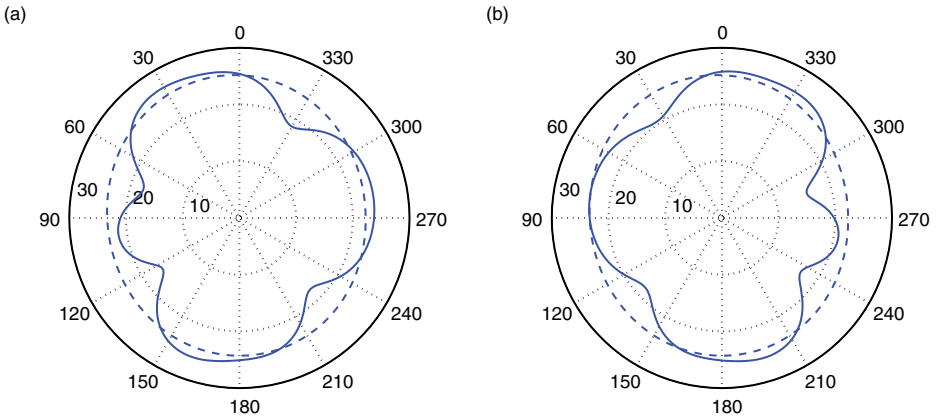

Figure 16: Same as figure 15, but for the second interaction tone.

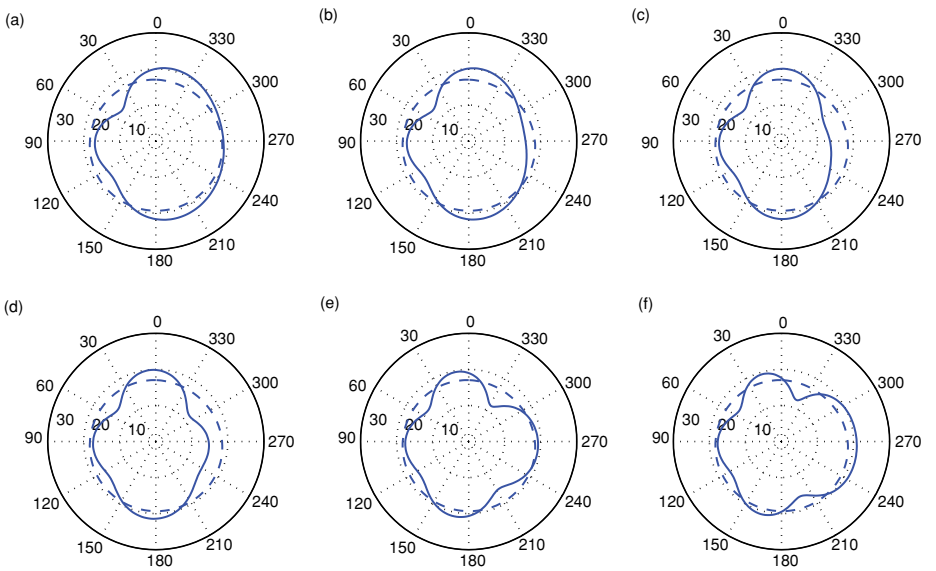

Figure 17: Far-field mean square pressure azimuthal directivity (in dB) of the first interaction tone at polar angle $\bar{\theta} = 45°$. The propeller is located at $\beta = 270°$. The distance between the rotor and fuselage is: (a) $b = 3.5r_t$, (b) $b = 4r_t$, (c) $b = 4.5r_t$, (d) $b = 5r_t$, (e) $b = 6r_t$ and (f) $b = 7r_t$. Key: solid line, with cylinder; dashed line, no cylinder.

to $7r_t$. The shielding effect of the cylinder at $\bar{\phi} = 90°$ is clearly observed in all the directivity plots. For the calculations which include the fuselage, the radiated pressure field displays a strong dependence on the distance between the rotor and the fuselage.

These results, in addition to those presented in figures 13 and 14 indicate that the noise produced by an installed open rotor is significantly affected by: (i) the location of the pylon, and, (ii) scattering from the fuselage. As such, it is likely that optimization of the pylon location and the location of the open rotor relative to the fuselage will significantly affect the level of the radiated sound field.

4. CONCLUSIONS

Analytic far-field solutions have been derived for a rotating ring of single-frequency monopole and dipole point sources located near to an infinite, rigid cylinder, in the presence of constant axial mean flow. It can be shown that the solutions for a rotating point source reduce to the comparable solutions for a stationary source, as the source's angular velocity $\Omega \rightarrow 0$[†]. Also, taking $M = 0$, solutions with no mean flow are recovered.

In addition, these far-field solutions have been extended to incorporate a distributed source model, in order to formulate a theoretical model which is more representative of an installed open rotor. The analytic solutions of the far-field pressure are expressed in terms of double or triple infinite summations of expressions containing Bessel functions. It can be shown using Debye's asymptotic expansion for $\mathrm{J}_{\nu}(\nu \operatorname{sech} \alpha)$, (see Ref. [12], Eq. 9.3.7, p. 366), that these summations convergence quite rapidly if $M_r = U_r/c_0$ is not too close to one. (M_r is the relative Mach number seen by an observer moving with the source.)

Illustrative results for the far-field pressure due to a rotating ring of point monopole sources located near an infinite, rigid cylinder show, as expected, that the direction of the rotation is important, viz-a-viz the locations of the cylinder and the rotor. The results show how the far-field pressure is affected by varying the source radius or the distance between the cylinder and the sources. Other parameters, such as the rotation speed, are also likely to affect the far-field pressure levels.

Additional illustrative results show predictions of the far-field pressure produced by periodic, unsteady loading on an installed open rotor. These provide more realistic examples of how the theory can be utilized to predict installed noise levels. Two different blade loading cases have been considered. The first corresponds to an 'impulsive' point force, which has maximum amplitude as the blade passes through the azimuthal angle $\phi = 0°$. It is hypothesized that this loading case produces a sound field which would be similar to that produced by the interaction of a pylon wake with a rotor blade. The incident sound field varies significantly with azimuthal location, and consequently the amplitude of the scattered sound field is highly dependent on the locations of the fuselage and the rotor. The second case investigated is a full calculation of the interaction of a pylon–wake with a rotor. Plots of the azimuthal directivity of the first two interaction tones are presented and the effect of cylinder scattering on the radiated field is clearly observed. A cursory investigation of the effect of the position of the rotor relative to the fuselage is also presented. It is shown that the azimuthal directivity of the scattered field varies strongly with rotor position.

[†]This requires, in some instances, further applications of Graf's Addition Theorem, and some significant algebraic manipulations.

ACKNOWLEDGEMENTS

Part of the work presented in this article was funded by the United Kingdom Technology Strategy Board project "SYMPHONY", coordinated by Rolls-Royce plc. The authors also wish to acknowledge the continuing financial support provided by Rolls-Royce plc through the University Technology Centre in Gas Turbine Noise at the Institute of Sound and Vibration Research.

REFERENCES

[1] D.B. HANSON and B. MAGLIOZZI. Propagation of propeller tone noise through a fuselage boundary layer. *Journal of Aircraft*, 22(1): 63–70, 1985.

[2] C.E. WHITFIELD, P.R. GLIEBE, R. MANI, and P. MUNGUR. High speed turboprop aeroacoustic study (single rotation) Vol. I: Model development. *NASA Contractor Report 182257*, May 1989.

[3] C.E. WHITFIELD, R. MANI, and P.R. GLIEBE. High speed turboprop aeroacoustic study (counter rotation) Vol. I – Model development. *NASA Contractor Report 185241*, July 1990.

[4] C.R. FULLER. Free-field correction factor for spherical acoustic waves impinging on cylinders. *AIAA Journal*, 27: 1722–1726, 1989.

[5] J.J. BOWMAN, T.B.A. SENIOR, and P.L.E. USLENGHI, editors. *Electromagnetic and Acoustic Scattering by Simple Shapes*. North-Holland Publishing Co. - Amsterdam, 1969.

[6] F.G. LEPPINGTON, M. BLAKEMORE, and K.H. HERON. The sound field due to a source moving along a helical path in the presence of a rigid cylinder. Submitted to the Journal of Sound and Vibration, 21 pages, 2008.

[7] S.A.L. GLEGG. Effect of centrebody scattering on propeller noise. *AIAA Journal*, 29: 572–576, 1991.

[8] M.J. KINGAN, C.J. POWLES, and R.H. SELF. Effect of centrebody scattering on open rotor noise. *AIAA Journal,* 48: 975–980, 2010.

[9] D.B. HANSON. Shielding of prop-fan cabin noise by the fuselage boundary layer. *Journal of Sound and Vibration*, 92(4): 591–598, 1984.

[10] H.Y. LU. Fuselage boundary-layer effects on sound propagation and scattering. *AIAA Journal*, 28:1180–1186, 1990.

[11] V.F. KOPIEV, A.A. MASLOV, and S.A. CHERNYSHOV Prop-Fan Sound Field Shielding by the Fuselage Boundary Layer. *DGLR/AIAA-92-02-068,*1992. DGLR/AIAA 14th Aeroacoustics Conference, Aachen, Germany, May 11–14, 5 pp.

[12] M. ABRAMOWITZ and I.A. STEGUN. *Handbook of Mathematical Functions*. Dover Publications, inc., New York, 1965.

[13] C.J. CHAPMAN. Similarity variables for sound radiation in a uniform flow. *Journal of Sound and Vibration*, 233: 157–164, 2000.

[14] S.W. RIENSTRA. Acoustic radiation from a semi-infinite annular duct in a uniform subsonic mean flow. *Journal of Sound and Vibration*, 94: 267–288, 1984.

[15] D.B. HANSON. Noise of counter-rotation propellers. *Journal of Aircraft*, 22: 609–617, 1985.

[16] A.B. PARRY. *Theoretical prediction of counter-rotating propeller noise*. PhD thesis, University of Leeds, Department of Applied Mathematical Studies, 1988.

[17] M.E. GOLDSTEIN. *Aeroacoustics*. McGraw-Hill, Inc., 1976.

[18] A.B. PARRY. Modular prediction scheme for blade row interaction noise. *Journal of propulsion and power*, 13: 334–341, 1997.